Dislocation Formation in Two-Phase Alloys

Akihiko Minami and Akira Onuki

Department of Physics, Kyoto University, Kyoto 606-8502, Japan

(Dated:)

Abstract

A phase field model is presented to study dislocation formation (coherency loss) in two-phase binary alloys. In our model the elastic energy density is a periodic function of the shear and tetragonal strains, which allows multiple formation of dislocations. The composition is coupled to the elastic field twofold via lattice misfit and via composition-dependence of the elastic moduli. By numerically integrating the dynamic equations in two dimensions, we find that dislocations appear in pairs in the interface region and grow into slips. One end of each slip glides preferentially into the softer region, while the other end remains trapped at the interface. Under uniaxial stretching at deep quenching, slips appear in the softer region and do not penetrate into the harder domains, giving rise to a gradual increase of the stress with increasing applied strain in plastic flow.

I. INTRODUCTION

In crystalline solids many kinds of phase transformations are strongly influenced by the elastic field[1,2,3,4]. Since the first work by Cahn[5,6] most theoretical studies have been focused on the coherent case in which the lattice planes are continuous through the interfaces. In the incoherent case, on the other hand, dislocations appear around the interfaces and the continuity is lost partially or even completely. Such incoherent microstructures emerge in various alloys when the lattice constants or the crystalline structures of the two phases are not close[7,8,9,10]. Moreover, they are produced in plastic flow because dislocations generated tend to be trapped at the interfaces. In particular, coherency loss has been extensivesly studied in the presence of γ' precipitates of the $L1_2$ structure[9,10].

Theory for the incoherent case is much more difficult than for the coherent case, obviously because the effects cannot be adequately described within the usual linear elasticity theory[11]. The aim of this paper is hence to present a simple mathematical model reasonably describing the incoherent effects in binary alloys. Use will be made of a recent nonlinear elasticity theory of plastic flow by one of the present authors[12].

A number of authors have studied composition changes around dislocations fixed in space and time, which lead to a compositional Cottrell atmosphere[13] or preferential nucleation around a dislocation[14,15]. As recent numerical work in two dimensions, phase separation has been studied by Léonard and Desai[16] and by Hu and Chen[17] using a continuum Ginzburg-Landau or phase field model in the presence of fixed dislocations. In these papers, dislocations preexist as singular objects before composition changes. We also mention atomistic simulations of dislocation motion influenced by diffusing solutes[18] or by precipitated domains[19].

Mechanical properties of two-phase solids are very different from those of one-phase solids[7,13,20]. In the presence of precipitated domains, dislocations can be pinned at the interface regions and networks of high-density dislocations can be formed preferentially in softer regions after deformations[9]. These effects are very complex but important in technology. Our simulations will give some insights on the behavior of dislocations in two-phase states.

This paper is organized as follows. In Section 2 we will present the free energy functional for the composition and the elastic field, in which the elastic energy density is a periodic

function of the tetragonal and shear strains and the composition is coupled to the elastic field. In Section 3 we will construct dynamical equations. In Section 4 numerical results will be given on the dislocation formation around domains and on the stress-strain relations under uniaxial stretching.

II. FREE ENERGY FUNCTIONAL

We consider a binary alloy consisting two components, A and B, neglecting vacancies and interstitials. The compositions, c_A and c_B, of the two components satisfy $c_A + c_B = 1$. In real metallic alloys undergoing a phase transition, there can be a change in the atomic configuration within unit cells as well as in the overall composition, resulting in ordered domains with the so-called $\mathrm{L1_0}$ or $\mathrm{L1_2}$ structure[2,4,21]. However, in this paper, the composition difference is the sole order parameter,

$$\psi = c_A - c_B, \tag{2.1}$$

for simplicity. The other variables representing the order-disorder phase transition are neglected. Then ψ is in the range $-1 \leqq \psi \leqq 1$ and

$$c_A = \frac{1}{2}(1+\psi), \quad c_B = \frac{1}{2}(1-\psi). \tag{2.2}$$

In our free energy $F = \int d\boldsymbol{r} f$ the order parameter ψ and the elastic displacement vector $\boldsymbol{u} = (u_x, u_y)$ are coupled. The free energy density f is of the form,

$$f = f_{\mathrm{BW}}(\psi) + \frac{C}{2}|\nabla\psi|^2 + \alpha e_1 \psi + f_{\mathrm{el}}. \tag{2.3}$$

The first term is the Bragg-Williams free energy density expressed as[4]

$$\begin{aligned} \frac{v_0}{k_{\mathrm{B}}T} f_{\mathrm{BW}} &= \frac{1+\psi}{2}\ln(1+\psi) + \frac{1-\psi}{2}\ln(1-\psi) \\ &- T_0\psi^2/2T, \end{aligned} \tag{2.4}$$

where v_0 is the volume of a unit cell representing the atomic volume, T_0 is the mean-field critical temperature in the absence of the coupling to the elastic field. If $|\psi| \ll 1$, we obtain the Landau expansion $v_0 f_{\mathrm{BW}}/k_{\mathrm{B}}T = (1 - T_0/T)\psi^2/2 + \psi^4/24 + \cdots$. However, we will not use this expansion form because we are interested in the deeply quenched case. The second term in (2.3) is the gradient term where C is a positive constant. The parameter

α represents the strength of the coupling between the composition and the dilation strain $e_1 = \nabla \cdot \boldsymbol{u}$. This coupling arises in the presence of a difference in the atomic sizes of the two species and is consistent with the empirical fact that the lattice constant changes linearly as a function of the average composition in many one-phase alloys (Vegard law). It gives rise to a difference in the lattice constants of the two phases in phase separation (lattice misfit). It also explains a composition inhomogeneity (Cottrell atmosphere in one-phase states or precipitate in two-phase states) around a dislocation.

In two dimensions $f_{\rm el}$ depends on the following strains,

$$\begin{aligned} e_1 &= \nabla_x u_x + \nabla_y u_y, \\ e_2 &= \nabla_x u_x - \nabla_y u_y, \\ e_3 &= \nabla_y u_x + \nabla_x u_y, \end{aligned} \tag{2.5}$$

where $\nabla_x = \partial/\partial x$ and $\nabla_y = \partial/\partial y$. The elastic displacement $\boldsymbol{u}$ is measured in a reference one-phase state at the critical composition. We call e_2 the tetragonal strain and e_3 the shear strain. In this paper we use a nonlinear elastic energy density of the form,

$$f_{\rm el} = \frac{1}{2} K e_1^2 + \Phi(\psi, e_2, e_3). \tag{2.6}$$

The first term represents the elastic energy due to dilation with K being the bulk modulus. The second term arises from anisotropic shear deformations defined for arbitrary values of e_2 and e_3. Assuming a square lattice structure[12], we set

$$\Phi = \frac{\mu_2}{4\pi^2}[1 - \cos(2\pi e_2)] + \frac{\mu_3}{4\pi^2}[1 - \cos(2\pi e_3)]. \tag{2.7}$$

The principal crystal axes are along or make angles of $\pm\pi/4$ with respect to the x or y axis. In Fig.1 we plot Φ as a function of e_2 and e_3 for the case $\mu_2 = \mu_3 = \mu_0$ in units of μ_0. If the system is homogeneous, elastic stability is attained for $\partial^2\Phi/\partial e_2^2 > 0$ and $\partial^2\Phi/\partial e_3^2 > 0$ or in the regions $|e_2 - n| < 1/4$ and $|e_3 - m| < 1/4$ with n and m being integer values[12].

For small strains $|e_2| \ll 1$ and $|e_3| \ll 1$, it follows the usual standard form[11],

$$\Phi \cong \frac{1}{2}\mu_2 e_2^2 + \frac{1}{2}\mu_3 e_3^2, \tag{2.8}$$

in the linear elasticity theory. Therefore,

$$\mu_2 = \frac{1}{2}(C_{11} - C_{12}), \quad \mu_3 = C_{44}, \tag{2.9}$$

in terms of the usual elastic moduli C_{11}, C_{12}, and C_{44}[11]. In the original theory[5] the isotropic linear elasticity with constant $\mu_2 = \mu_3$ was assumed. Subsequent theories treated the case of the cubic linear elasticity with constant μ_2 and μ_3[2,3,4,6,22]. In the present paper, while K is a constant, μ_2 and μ_3 depend on the composition as

$$\mu_2 = \mu_{20} + \mu_{21}\psi, \quad \mu_3 = \mu_{30} + \mu_{31}\psi. \tag{2.10}$$

If $\mu_{21} > 0$ and $\mu_{31} > 0$, the regions with larger (smaller) ψ are harder (softer) than those with smaller (larger) ψ. It is known that this *elastic inhomogeneity* gives rise to asymmetric elastic deformations in two-phase structures and eventual pinning of the domain growth[4,23,24].

In our theory $\Phi(\psi, e_2, e_3)$ in (2.7) is the simplest periodic function of e_2 and e_3 with period 1. The periodicity arises from the fact that the square lattice is invariant with respect to a slip of the crystal structure by a unit lattice constant along a line parallel to the x or y axis. Notice that, under rotation of the reference frame by θ, e_2 and e_3 are changed to e_2' and e_3', respectively, with[12]

$$\begin{aligned} e_2' &= e_2 \cos 2\theta + e_3 \sin 2\theta, \\ e_3' &= -e_2 \sin 2\theta + e_3 \cos 2\theta. \end{aligned} \tag{2.11}$$

For $\theta = \pi/2$ we have $e_2' = -e_2$ and $e_3' = -e_3$, so $f_{\rm el}$ in (2.7) remains invariant. For $\theta = \pi/4$ we have $e_2' = e_3$ and $e_3' = -e_2$ and recognize that the roles of tetragonal and shear strains are exchanged. For $\mu_2 = \mu_3$, the linear elasticity in (2.8) becomes isotropic, but the nonlinear elasticity is still anisotropic (from the fourth-order terms in the expansion of Φ in (2.7) in powers of e_2 and e_3).

The elastic stress tensor $\overleftrightarrow{\sigma} = \{\sigma_{ij}\}$ is expressed as

$$\begin{aligned} \sigma_{xx} &= Ke_1 + \alpha\psi + \mu_2 \sin(2\pi e_2)/2\pi, \\ \sigma_{yy} &= Ke_1 + \alpha\psi - \mu_2 \sin(2\pi e_2)/2\pi, \\ \sigma_{xy} &= \sigma_{yx} = \mu_3 \sin(2\pi e_3)/2\pi. \end{aligned} \tag{2.12}$$

In the linear elasticity, $\sin(2\pi e_2)/2\pi$ and $\sin(2\pi e_3)/2\pi$ are replaced by e_2 and e_3, respectively. Notice the relation,

$$\nabla \cdot \overleftrightarrow{\sigma} = -\frac{\delta}{\delta \boldsymbol{u}} F, \tag{2.13}$$

where ψ is fixed in the functional derivative $\delta F/\delta \boldsymbol{u}$.

The mechanical equilibrium condition $\nabla\cdot \overleftrightarrow{\sigma}= \mathbf{0}$ is equivalent to the extremum condition $\delta F/\delta \boldsymbol{u} = \mathbf{0}$. In the coherent case this condition may be assumed even in dynamics. In fact, using this condition in the linear elasticity, the elastic field has been expressed in terms of ψ in the previous theories (see the appendix)[1,2,3,4,5,6]. We then find the following. (i) The typical strain around domains is given by[4]

$$e_0 = \alpha \Delta c/L_0, \tag{2.14}$$

where $\Delta c = \Delta\psi/2$ is the composition difference between the two phases and

$$L_0 = K + \mu_{20} \tag{2.15}$$

is the longitudinal elastic modulus. This strain needs to be small ($e_0 < 1/4$ approximately) as long as the system stays in the coherent regime. (ii) As will be shown in the the appendix, in the limit of weak cubic elasticity and weak elastic inhomogeneity, one-phase states become linearly unstable for $k_{\rm B}[T - T_0 + T\langle\psi\rangle^2/2]/v_0 < \alpha^2/L_0$. At the critical composition $\langle\psi\rangle = 0$ this condition becomes $T < T_{\rm s}$ with

$$T_{\rm s} = T_0 + v_0\alpha^2/L_0 k_{\rm B}. \tag{2.16}$$

(iii) Furthermore, (A.5) suggests that the typical domain size in steady pinned states is a decreasing function of the quench depth $T_{\rm s} - T$.

III. DYNAMIC EQUATIONS

In the incoherent case the mechanical equilibrium does not hold around dislocation cores when dislocations are created and when they are moving[12]. We thus need to set up the dynamic equation for the elastic displacement $\boldsymbol{u}$. In this paper the lattice velocity $\boldsymbol{v} = \partial\boldsymbol{u}/\partial t$ obeys the momentum equation[11],

$$\rho\frac{\partial \boldsymbol{v}}{\partial t} = \eta_0\nabla^2\boldsymbol{v} + \nabla\cdot \overleftrightarrow{\sigma}\ . \tag{3.1}$$

The mass density ρ and the shear viscosity η_0 are constants. We neglect the bulk viscosity term ($\propto \nabla\cdot\boldsymbol{v}$) in (3.1) for simplicity[12]. In our model the sound waves relax owing to this viscous damping and the mechanical equilibrium $\nabla\cdot \overleftrightarrow{\sigma}= \mathbf{0}$ is rapidly attained unless η_0 is very small. Note that the nonlinear terms in (3.1) are only those in σ_{ij} in (2.12).

The composition obeys the diffusive equation,

$$\frac{\partial \psi}{\partial t} = \nabla \cdot \lambda(\psi) \nabla \frac{\delta F}{\delta \psi}. \tag{3.2}$$

The kinetic coefficient depends on ψ as[25,26]

$$\lambda(\psi) = \lambda_0 (1 - \psi^2) = 4\lambda_0 c_A c_B, \tag{3.3}$$

where λ_0 is a constant. Here $\boldsymbol{u}$ is fixed in the chemical potential difference $\delta F/\delta\psi$, so

$$\begin{aligned} \frac{\delta F}{\delta \psi} &= \frac{k_{\rm B}}{v_0}\Big[\frac{T}{2}\ln\Big(\frac{1+\psi}{1-\psi}\Big) - T_0\psi\Big] - C\nabla^2\psi + \alpha e_1 \\ &+ \frac{\mu_{21}}{4\pi^2}[1-\cos(2\pi e_2)] + \frac{\mu_{31}}{4\pi^2}[1-\cos(2\pi e_3)]. \end{aligned} \tag{3.4}$$

The last two terms arise from the elastic inhomogeneity. If $\lambda(\psi)$ is of the form of (3.3), the diffusion equation $\partial c_A/\partial t = D_0 \nabla^2 c_A$ ($\partial c_B/\partial t = D_0 \nabla^2 c_B$) follows in the dilute limit $c_A \to 0$ ($c_B \to 0$) with

$$D_0 = \lambda_0 k_{\rm B} T v_0^{-1}, \tag{3.5}$$

where the coupling to the elastic field becomes negligible. In usual solid mixtures the diffusion is very slow and vacancies are in many cases crucial for a microscopic description of diffusion[26]. Effects of such point defects are not treated in the present theory.

The total free energy $F_{\rm tot} = F + \int d\boldsymbol{r} \rho \boldsymbol{v}^2/2$ including the kinetic energy then changes in time as

$$\frac{d}{dt} F_{\rm tot} = -\int d\boldsymbol{r} \Big[\sum_{ij} \eta_0 (\nabla_i v_j)^2 + \lambda(\psi) \Big| \nabla \frac{\delta F}{\delta \psi} \Big|^2 \Big]. \tag{3.6}$$

Here the surface integrals have been omitted, which vanish if the boundaries are fixed and there is no flux of the atoms from outside (and also if the periodic boundary condition is imposed in simulations). The above time-derivative is non-positive-definite. As a result, the equilibrium is attained when $\boldsymbol{v} = \nabla \cdot \overleftrightarrow{\sigma} = \boldsymbol{0}$ and $\delta F/\delta\psi$ =const.

If the lattice is deformed significantly, we should add the convective term $-\nabla(\psi \boldsymbol{v})$ on the right hand side of (3.2), treating (3.2) as the equation in the Euler description. If its presence is assumed, another term of the form, $-\psi \nabla \delta F/\delta\psi$, becomes also needed on the right hand side of (3.1). With these two terms we again have $dF_{\rm tot}/dt \leqq 0$. These two terms are well-known in critical dynamics of fluids[4]. However, in our solid case, the magnitude of the displacement $\Delta \boldsymbol{u} = \int_0^t dt' \boldsymbol{v}(\boldsymbol{r}, t')$ remains small and these two terms give rise to no essential differences in our results at not large applied strains[27].

Also note that the dynamic equations (3.2) and (3.3) may be treated as Langevin equations with addition of the random noise terms related to the kinetic coefficients $\lambda(\psi)$ and η_0 via the fluctuation-dissipation relations[4]. In this paper, however, we neglect the random noise, because the thermal energy $k_{\rm B}T$ will be assumed to be much smaller than the typical energy of elastic deformations.

IV. NUMERICAL RESULTS

A. Method

We integrated (3.1) and (3.2) in two dimensions on a 256×256 square lattice. The mesh size Δx was set equal to the lattice constant a in the reference state with $\boldsymbol{u} = \boldsymbol{0}$, so the system length is $L_0 = 256a$. The vectors, $\boldsymbol{u}$ and $\boldsymbol{v}$, are defined at the lattice points (n, m), while the strains, the tensors, and the composition are defined on the middle points $(n+1/2, m+1/2)$. These are needed to realize well-defined microscopic slips in our numerical scheme[12]. The periodic boundary condition was imposed except the simulation of applying uniaxial deformation (Figs.13 and 14). Because the time scale of $\boldsymbol{u}$ is shorter than that of ψ, we integrated (3.1) using an implicit Crank-Nicolson method. Space and time will be measured in units of a and

$$\tau_0 = (\rho/\mu_{20})^{1/2} a, \tag{4.1}$$

respectively, where μ_{20} is defined by (2.10) and $(\mu_{20}/\rho)^{1/2}$ is the transverse sound velocity propagating in the [11] direction. The free energies and the free energy densities are measured in units of $\mu_{20}a^2$ and μ_{20}, respectively. For simplicity, the scaled time $\tau_0^{-1}t$, position vector $a^{-1}\boldsymbol{r}$, and displacement vector $a^{-1}\boldsymbol{u}$ will be written as t, $\boldsymbol{r}$, and $\boldsymbol{u}$, respectively, in the same notation.

In this paper we set $K/\mu_{20} = 4.5$, $\alpha/\mu_{20} = 0.6$, and $k_{\rm B}T_0/v_0\mu_{20} = 0.05$, where T_0 is the mean-field critical temperature in (2.4). Since $T \sim T_0$ hereafter, the elastic energy to create a single slip ($\sim \mu_{20}v_0$) is much larger than $k_{\rm B}T$ in our simulations. Furthermore, we assume weak cubic elastic anisotropy with $\mu_{30}/\mu_{20} = 1.1$ and moderate elastic inhomogeneity with $\mu_{21} = \mu_{31} = 0.6\mu_{20}$.

The dimensionless kinetic coefficients are given by

$$\lambda_0^* = \lambda_0\tau_0\mu_{20}a^{-2}, \quad \eta_0^* = \eta_0/\tau_0\mu_{20}. \tag{4.2}$$

We set $\lambda_0^* = 0.001$ and $\eta_0^* = 0.1$. Then,

$$\lambda_0^*/\mu_0^* = D_0\rho/\eta_0 \sim 10^{-2}. \tag{4.3}$$

Since the relaxation rate of a sound with wave number k is $\eta_0 k^2/\rho$, the time scale of ψ becomes longer than that of the elastic field by two orders of magnitude. In real solid alloys, these two time scales are much more distinctly separated, probably except for hydrogen-metal systems where the protons diffuse quickly[4].

In homogeneous one-phase states we have $e_2 = e_3 = 0$ and $e_1 = -\alpha\psi/K$. Here well-known is a parameter $\eta = |\partial a/\partial\psi|/a$ representing the strength of the composition-dependence of the lattice constant a in a mixture[5]. In our case we have $\eta = \alpha/2K = 0.067$ and the spinodal temperature $T_{\rm s}$ in (2.16) becomes 2.31.

B. Slips and composition changes

Edge dislocations appear in the form of slips or dipole pairs[12], because a single isolated dislocation requires a very large elastic energy. Slips are thus fundamental units of plastic deformations. In Fig.2 we show the displacement and the composition around typical slips in a one-phase steady state with length $10\sqrt{2}a$ in the upper plate and $10a$ in the lower plate. Here we initially prepared a slip given by the linear elasticity theory[12] at the critical composition ($\langle\psi\rangle = 0$) and let $\boldsymbol{u}$ and ψ relax until the steady state was achieved. The temperature was kept at $T/T_0 = 2.5$ and no phase separation occurred. As in the previous simulations[17,18], we can see Cottrell atmospheres around the dislocation cores. The maximum and minimum of ψ at the lattice points close to the dislocation cores are of order ± 0.6. Cottrell's result is obtained as follows: Let T be much higher than T_0 and α^2/L_0 and the gradient term be neglected; then, the condition $\delta F/\delta\psi$ =const. yields $c_A/(1-c_A)$ =const. $\exp(-U/k_{\rm B}T)$, where $U = v_0\alpha{e_1}^{28}$. In our case the maximum of $|U|/k_{\rm B}T$ at the lattice points is of order 1 and the accumulation is not very strong.

As a next step, starting with the configuration in Fig.2, we lowered the temperature to $T/T_0 = 2$ to induce spinodal decomposition. Subsequently the Cottrell atmospheres grew into domains and the dislocation cores stayed at the interface regions. The domain size attained finally was of order $50a$. Fig.3 illustrates the displacement and the composition in the final steady state, where the maximum and minimum of ψ are about ± 0.9. Léonard and

Desai[16] obtained similar composition profiles in spinodal decomposition, where the elastic field of dislocations (given by the linear elasticity theory) was fixed in space and time.

Mathematically, slips in steady states satisfy $\delta F/\delta \boldsymbol{u} = \boldsymbol{0}$ and $\delta F/\delta\psi$ =const. Without externally applied strains, they are metastable owing to the Peierls potential energy arising from the discreteness of the lattice structure[12]. Although not discussed in this paper, slips become unstable against expansion or shrinkage with increasing applied strain.

C. Dislocation formation around a hard domain

Fig.4 shows a single large hard (A-rich) domain at the center in the coherent condition at shallow quenching $T/T_0 = 2$ after a long equilibration time. Here ψ is about 0.7 inside the domain and about -0.7 outside it. Its shape slightly deviates from sphericity owing to the weak cubic anisotropy assumed in this paper. We next performed a second deeper quenching to $T/T_0 = 1$. Subsequent diffusional adjustment of the composition proceeded very slowly, but a discontinuity of the order parameter $\Delta\psi$ about 1.8 was established relatively rapidly across the interface[4]. As a result, at a time about 1000 after the second quenching, the maximum of $|e_2|$ reached 1/4, the value at the stability limit, in the interface region (see the sentences below (2.7)). We then observed formation of dislocations and generation of sound waves emitted from the dislocations. The upper panel of Fig.5 shows the coherent elastic displacement $\boldsymbol{u}_{\rm coh}$ just before the dislocation formation, while the lower panel shows the subsequent additional incoherent change $\delta\boldsymbol{u} = \boldsymbol{u} - \boldsymbol{u}_{\rm coh}$ after a time interval of 1000. The free energy F in the state in the lower panel is smaller than that in the upper panel by 152.9 in units of $\mu_{20}a^2$. More details are as folllows: (i) two pairs of dislocation dipoles (four dislocations) appeared simultaneously in a narrow region, (ii) two of them glided preferentially into the softer region forming two slips perpendicular to each other, and (iii) slips collided in many cases and stopped far from the droplet, resulting in a nearly steady elastic deformation. Thus a half of the dislocation cores stayed at the interface and the others were distributed around the domain. These three processes took only a short time of order 100.

After the above dislocation formation at a relatively early stage, the composition changed very slowly. We show three figures at $t = 23000$. In Fig.6 we displays the following strain,

$$e = (e_2^2 + e_3^2)^{1/2}, \tag{4.4}$$

which is invariant with respect to the rotational transformation (2.11). The slips make an angle of $\pm\pi/4$ with respect to the x axis in the regions with large $|e_2|$ (in the uniaxially deformed regions), while they are parallel to the x or y axis in the corner regions with large $|e_3|$[12]. We also notice that the dislocation formation took place with the symmetry axis in the [11] direction for our special geometry. Fig.7 gives the free energy density f in (2.3), where the peaks outside the domain represent the dislocation cores. In the interface region it exhibits a cliff-like structure arising from the gradient term and higher peaks arising from the dislocation cores. Fig.8 shows the order parameter ψ, where we can see Cottrell atmospheres around the dislocation cores surrounding the domain. The system is still transient and there is still a small composition flux through the interface.

D. Dislocation formation in a soft network

Next we examine dislocation formation when hard rectangular domains are densely distributed and wrapped by a percolated soft network. As in Fig.9, we prepared such a steady domain structure at $T/T_0 = 2$ in the coherent condition. As in the previous simulations[23,24], the hard domains (in gray) are elastically isotropic, while the soft network (in white) is mostly uniaxially stretched. That is, in the soft stripes between the two adjacent hard domains, we obtain $e_2 \sim 0.2$ in the horizontal stripes and $e_2 \sim -0.2$ in the vertical stripes. We then quenched T to $T/T_0 = 1$ to induce the composition readjustment. Fig.10 displays the resultant time evolution of the total free energy $F = \int d\boldsymbol{r} f$ and the snapshots of e in (4.4) at the points A, $\cdots$, and E. It demonstrates that F mainly decreases due to the composition change but sometimes due to appearance and gliding of slips in the soft stripes. Note that the overall composition adjustment occurs slowly on the time scale of $R^2/D_0 = 10^5 - 10^6$ where R is the domain size. In Fig.11 we show the displacement $\boldsymbol{u}$ within the square window in B, C and D, respectively, while in Fig.12 the bird views of the free energy density f the square window are given at $t = 0$ and 4475 after the second quench. Fig.12 clearly illustrates appearance of the peaks representing the dislocation cores.

E. Uniaxial stretching in two-phase states

Finally we apply a constant uniaxial deformation to initially coherent states with $\langle\psi\rangle = 0$ to induce plastic flow. That is, we set $u_x = u_y = 0$ at the bottom ($y = 0$) and $u_x = -u_y = \epsilon L_0/2$ at the top ($y = L_0$). The applied strain rate was fixed at $\dot{\epsilon} = 10^{-4}$, so $\epsilon = \dot{\epsilon}t$ with t being the time after application of the deformation. In Fig.13 we plot the average normal stress N_1 vs the applied strain ϵ for $T/T_0 = 3$, 2.4, and 2 (upper plate), where

$$N_1 = \langle\sigma_{xx} - \sigma_{yy}\rangle = \frac{1}{\pi}\langle\mu_2 \sin(2\pi e_2)\rangle, \tag{4.5}$$

where $\langle\cdots\rangle$ denotes taking the spatial average. The snapshots of e in (4.4) are also given at the points a, b, and c (lower plates). For $T/T_0 = 3$ the system is in a homogeneous one-phase state and random numbers with variance 0.01 were assigned to ψ at the lattice points at $t = 0$. In the initial state at $T/T_0 = 2.4$ the maximum and minimum of ψ and e_2 are ± 0.32 and ± 0.05, respectively. At $T/T_0 = 2$ these numbers are magnified to ± 0.75 and ± 0.20. All the initial states are coherent without dislocations. For $T/T_0 = 3$ the elastic instability occurs at $\epsilon = 1/4$ resulting in a fine mesh of slips as in the lower left plate. For $T/T_0 = 2.4$ the onset point of the slip formation is decreased to $\epsilon = 0.17$. For $T/T_0 = 3$ the onset is very early at 0.015, the stress-strain relation exhibits zig-zag behavior upon appearance of slips, and the stress continue to increase on the average (up to the upper bound of ϵ given by 0.35 in the simulation). Fig.14 consists of snapshots of e in (4.4) and the shear deformation energy density Φ in (2.7) in units of μ_{20}. We can see quadratic appearance of dislocations at the center of the uniaxially stretched stripes at $\epsilon = 0.05$ (top plate), gliding of the dislocations and pinning at the interfaces at $\epsilon = 0.1$ (top and middle plates), and thickening of the slips into *shear bands* at $\epsilon = 0.2$ (bottom plate).

We mention a creep experiment in the presence of high volume fractions of γ' precipitates[9], where softer disordered γ regions were observed to be filled with dislocation networks after large deformations.

V. SUMMARY AND CONCLUDING REMARKS

In summary, we have presented a coarse-grained phase field model of plastic deformations in two-phase alloys. Though our simulations have been performed in two dimensions, a number of insights into the very complex processes of plasticity have been gained. We

mention them and give some remarks.

(i) Performing a two-step quench, we have numerically examined dislocation formation around the interface regions, which occur spontaneously in deeply quenched phase separation. Experimentally[10], dislocation formation has been observed around growing $\gamma'(Al_3Sc)$ precipitates at low volume fractions when the radii exceeded a threshold about 20nm. Such spontaneous dislocation formation with domain growth has not yet been studied theoretically.

(ii) We have found that dislocations glide preferentially into the softer regions with smaller shear moduli and tend to be trapped in the interface regions in agreement with a number of observations[7]. Theoretically, the composition-dependence of the elastic moduli (elastic inhomogeneity) is a crucial ingredient to explain the experiments.

(iii) We have applied uniaxial strain to create multiple slips in two-phase alloys which were initially in the coherent condition. The dislocation formation starts in the mostly stretched middle points of the soft stripes. A stress-strain curve in Fig.13 at deep quenching is very different from the curves in one-phase states. In real two-phase alloys, a similar monotonic increase of the stress without overshoot has been observed, but a considerable amount of defects should preexist in such experiments particularly in work-hardened samples[7,13,20].

This work is a first theoretical step to understand complex phenomena of incoherency in solids. Finally, we mention two future problems which could be studied numerically in our scheme.

(i) The composition has been taken as a single order parameter. Extension of our theory is needed to more general phase separation processes involving an order-disorder phase transition[2,4,16] and to diffusionless (Martensitic) structural phase transitions[2,4].

(ii) Dislocations move under applied strain. The motion is complicated when they are coupled with an order parameter and when the time scale of the order parameter is slow[18,29].

Acknowledgments

We would like to thank Toshiyuki Koyama for valuable discussions on the incoherency effects in metallic alloys. This work is supported by Grants in Aid for Scientific Research and for the 21st Century COE project (Center for Diversity and Universality in Physics) from the Ministry of Education, Culture, Sports, Science and Technology of Japan.

Appendix

Here we assume weak elastic anisotropy and weak elastic inhomogeneity in the coherent condition in two dimensions, supposing shallow quenching. Then we may eliminate the elastic field in terms of ψ using the mechanical equilibrium condition $\nabla \cdot \overleftrightarrow{\sigma} = \mathbf{0}$ in the linear elasticity. We consider the space integral of the last two terms in the free energy density in (2.3): $\Delta F = \int d\boldsymbol{r}[\alpha e_1 \psi + f_{\rm el}]$. We assume that $|\mu_{21}|$ and $|\mu_{31}|$ are much smaller than $L_0 = K + \mu_{20}$ and that $\xi_a = 2(\mu_{20}/\mu_{30} - 1)$ is small. Then ΔF may be rewritten as[4,23,24]

$$\begin{aligned} \Delta F \;&=\; \int d\boldsymbol{r}\Big[-\frac{\alpha^2}{2L_0}\psi^2 + \frac{1}{2}\tau_{\rm cub}|\nabla_x\nabla_y w|^2\Big] \\ &+\; \int d\boldsymbol{r}\Big[g_2\psi|(\nabla_x^2 - \nabla_y^2)w|^2 + g_3\psi|\nabla_x\nabla_y w|^2\Big], \end{aligned} \tag{A.1}$$

where w is obtained from the Laplace equation,

$$\nabla^2 w = \psi - \langle\psi\rangle, \tag{A.2}$$

with $\langle\psi\rangle$ being the average order parameter. In the first line of (A.1) the bilinear terms are written with

$$\tau_{\rm cub} = -(2\alpha^2/L_0^2)\mu_{20}\xi_a. \tag{A.3}$$

The term proportional to $\tau_{\rm cub}$ gives rise to anisotropic domains[22]. The second line consists of the third-order terms with

$$g_2 = \mu_{21}\alpha^2/2L_0^2, \quad g_3 = 2\mu_{31}\alpha^2/L_0^2. \tag{A.4}$$

The third-order terms are known to give rise to pinning of domain growth (and some frustration effects when g_2 and g_3 have different signs)[23,24].

In our simulations we set $\xi_a = 2(1/1.1-1) \cong -0.18$ and $\tau_{\rm cub} \cong 0.0043\mu_{20}$, so the domains tend to become square or rectangular with interfaces parallel to the x or y axis. Furthermore, we set $g_2 = g_3/4 \cong 0.0035\mu_{20}$. For $\mu_{21} \sim \mu_{31}$ the typical domains in pinned two-phase states $R_{\rm E}$ is given by[23]

$$R_{\rm E} \sim \gamma/[\mu_{21}(\Delta c)^3], \tag{A.5}$$

where γ is the surface tension and Δc is the composition difference between the two phases.

Thus $R_{\rm E}$ decreases as the quenching becomes deeper.

---

[1] J.W. Cahn, in *Critical Phenomena in Alloys, Magnets, and Superconductors*, edited by R.I. Jafee *et al.* (McGraw-Hill, New York, 1971), p.41.

[2] A.G. Khachaturyan, *Theory of Structural Transformations in Solids* (John Wiley & Sons, New York, 1983).

[3] P. Fratzl, O. Penrose, and J.L. Lebowitz, J. Stat. Phys. **95**, 1429 (1999).

[4] A. Onuki, *Phase Transition Dynamics* (Cambridge University Press, Cambridge, 2002).

[5] J.W. Cahn, Acta Metall. **9**, 795 (1961).

[6] J.W. Cahn, Acta Metall. **11**, 1275 (1963).

[7] J.L. Strudel, in *Physical Metallurgy*, edited by R.W. Cahn and P. Haasen (North-Holland, Amsterdam, 1996), p.2106.

[8] E. Nembach, *Particle Strengthening of Metals and Alloys* (Wiley, New York,1997).

[9] T. M. Pollock and A. S. Argon, Acta Mater. **40**, 1 (1992).

[10] E. A. Marquis and D. N. Seidman, Acta Mater. **48**, 3477 (2000); M.J. Jones and F.J. Humphreys, ibid. **51**, 2149 (2003); S.Iwamura and Y. Miura, ibid. **52**, 591 (2004).

[11] L.D. Landau and E.M. Lifshitz, *Theory of Elasticity* (Pergamon, New York, 1973).

[12] A. Onuki, Phys. Rev. E **68**, 061502 (2003). In this paper a triangular lattice is assumed in two dimensions.

[13] A.H. Cottrell, *Dislocations and Plastic Flow in Crystals* (Clarendon Press, Oxford, 1953) ; A.H. Cottrell and M.A. Jaswon. Proc. R. Soc. A **199**, 104 (1949).

[14] J.W. Cahn, Acta Metall. **5**, 160 (1957).

[15] A. A. Boulbitch and P. Tolédano, Phys. Rev. Lett. **81**, 838 (1998).

[16] F. Léonard and R. Desai, Phys. Rev. B, **58**, 8277 (1988).

[17] S.Y. Hu and L.Q. Chen, Acta Mater. **49**, 463 (2001); Comput. Mater. Sci. **23**, 270 (2002).

[18] Y. Wang, D. J. Srolovitz, J. M. Rickman and R. LeSar, Acta Mater., **48**, 2163 (2000).

[19] S.Y. Hu, S.Schmauder, and L.Q. Chen, Phys. Status Solidi. B **220**, 845 (2000).

[20] A.S. Argon, in *Physical Metallurgy*, edited by R.W. Cahn and P. Haasen (North-Holland, Amsterdam, 1996), p.1878, 1958; P. Haasen, ibid. p.2010.

[21] C. Sagui, A. M. Somoza and R.C. Desai, Phys. Rev. E **50**, 4865 (1994).

[22] H. Nishimori and A. Onuki, Phys. Rev. B **42**, 980 (1990).

[23] A. Onuki and H. Nishimori, Phys. Rev. B **43**, 13649 (1991); A. Onuki and A. Furukawa, Phys. Rev. Lett. **86**, 452 (2001).

[24] D. Orlikowski, C. Sagui, A. M. Somoza and C. Roland, Phys. Rev. B **59**, 8646 (1999); ibid. **62**, 3160 (2000).

[25] K. Kitahara and M. Imada, Prog. Theor. Phys. Suppl. **64**, 65 (1978).

[26] K. Binder, in *Material Sciences and Technology* ed. R. W. Cohen, P. Haasen and E.J. Kramer (VCH, Weinheim, 1991), Vol. 5.

[27] In simulations with these terms the time mesh size Δt must be made very small when dislocations are formed. Such attempts (in the uniaxial deformation case in Figs.13 and 14) did not essentially alter the results.

[28] The linear elasticity theory[11] yields $e_1 = \text{const.}y/(x^2 + y^2)$ for a single edge dislocation at the origin. The expression for a slip is obtained in the presence of two dislocations with opposite Burgers vectors. See Ref.[10].

[29] A. L. Korzhenevskii, R. Bausch, and R. Schmitz, Phys. Rev. Lett. 91, 236101 (2003).

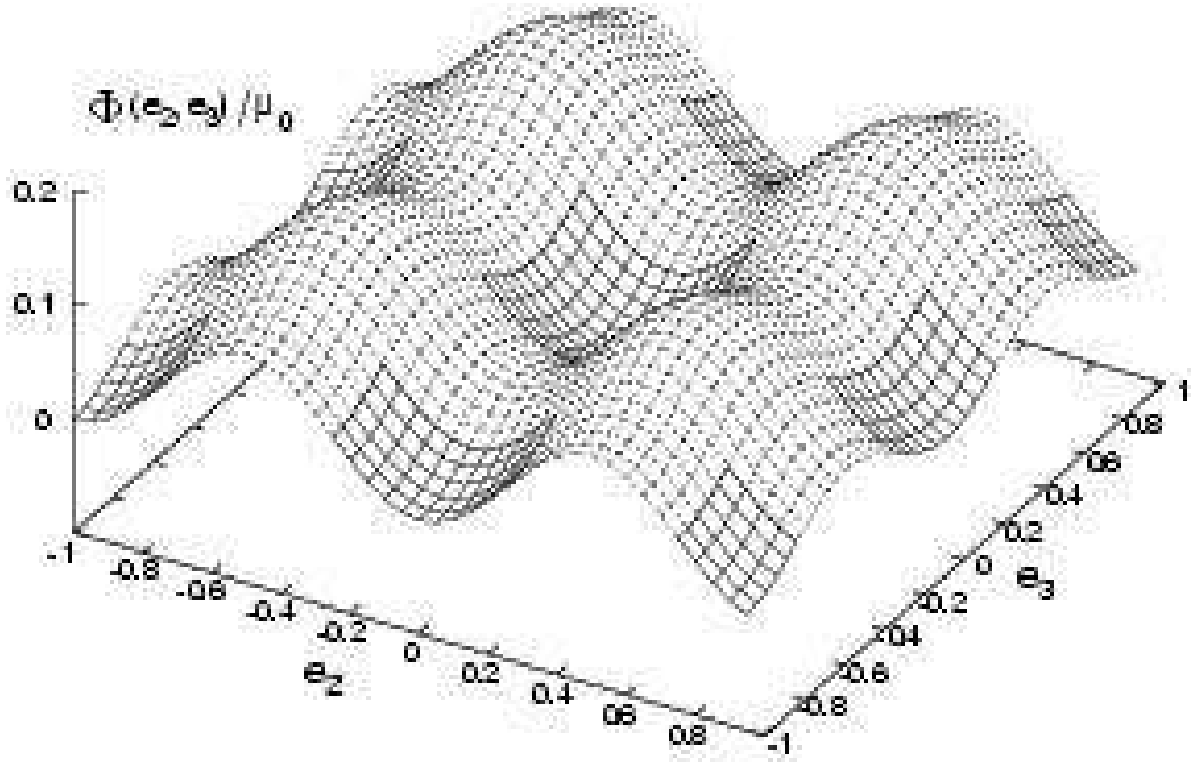

FIG. 1: Normalized shear deformation energy $\Phi(e_2, e_3)/\mu_0$ for the case $\mu_2 = \mu_3 = \mu_0$. The elastically stable regions are meshed with solid lines on the surface.

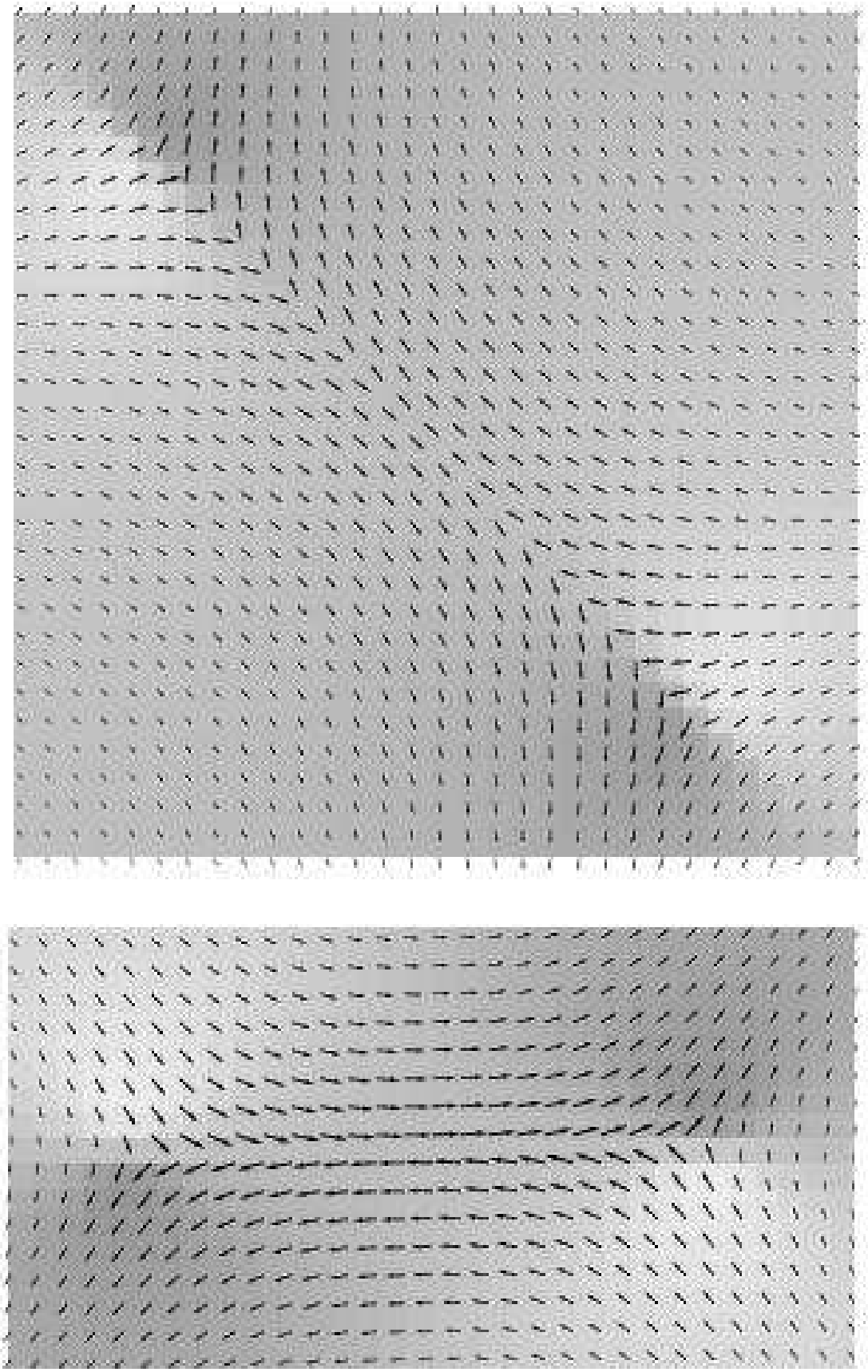

FIG. 2: Displacement vector for a slip (dislocation pair) making an angle of $3\pi/4$ (upper plate) and 0 (lower plate) with respect to the x (horizontal) axis in a one-phase steady state at $T/T_0 = 2.5$. The arrows are from the initial position in a perfect crystal to the deformed position. The degree

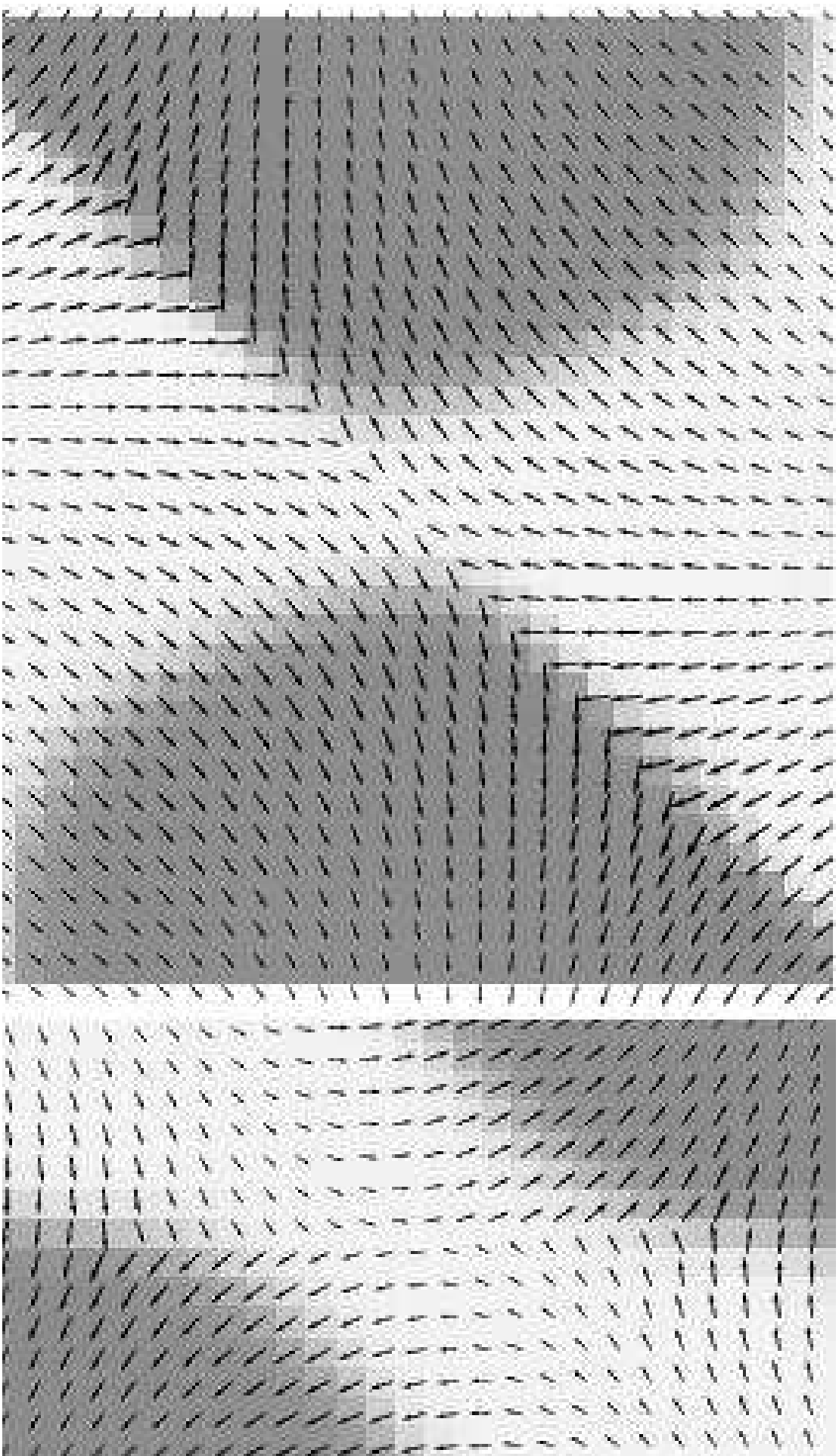

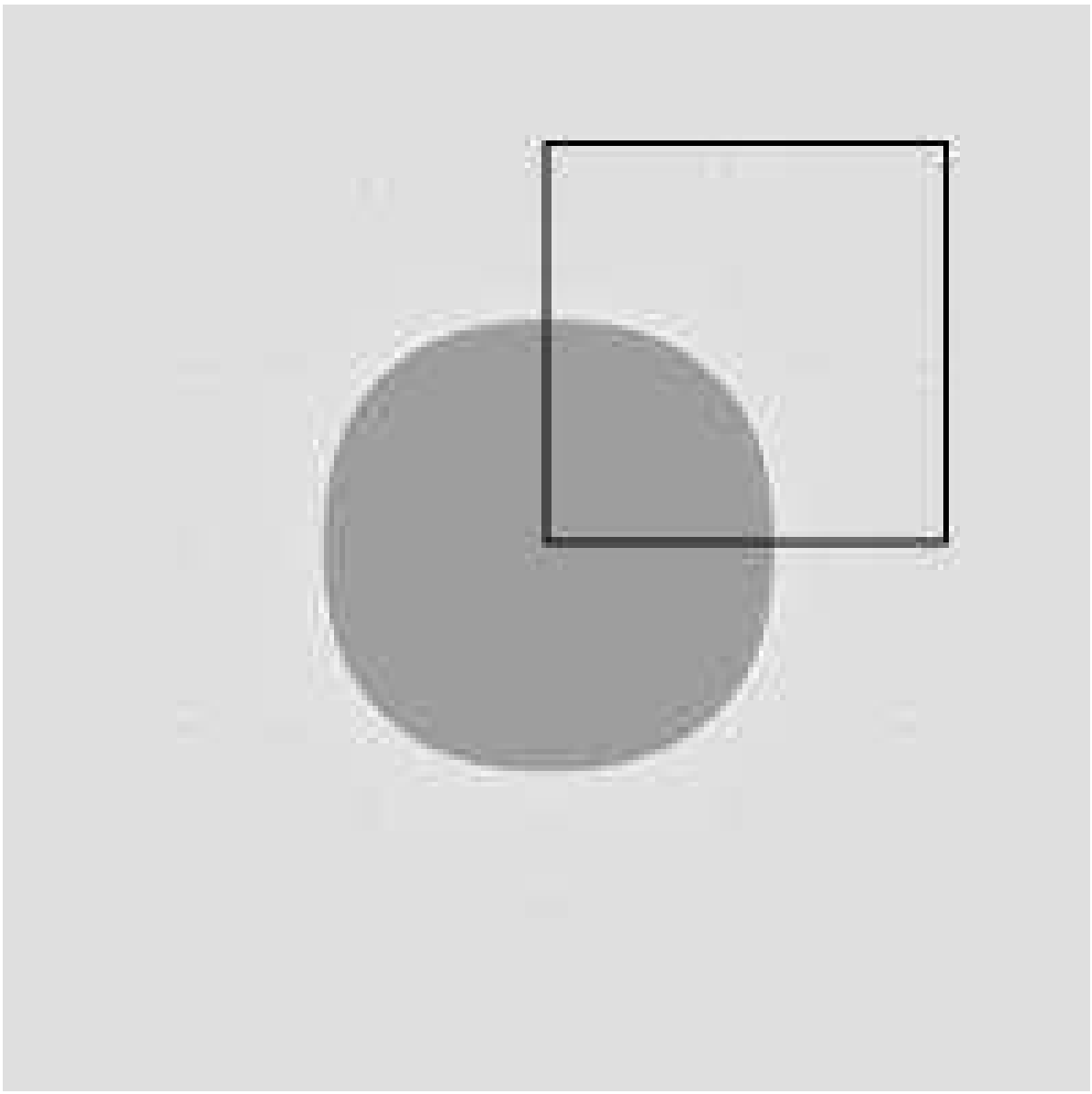

FIG. 4: Hard domain in a steady state at $T/T_0 = 2$. The displacement in the square region will be displayed in Fig.5.

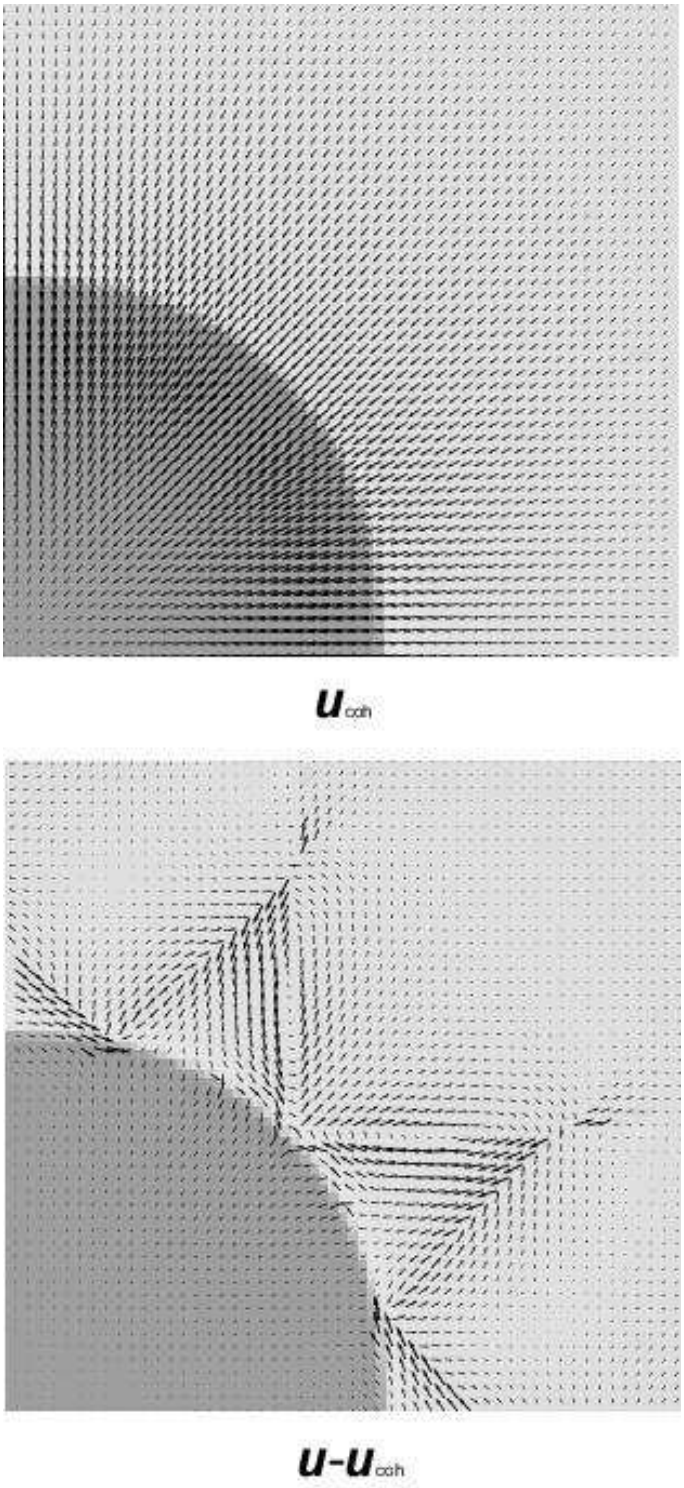

FIG. 5: Upper plate: Coherent elastic displacement $\boldsymbol{u}_{\rm coh}$ just before birth of dislocations at deep quenching at $T/T_0 = 1$. Right: Incoherent elastic displacement after appearance of dislocations.

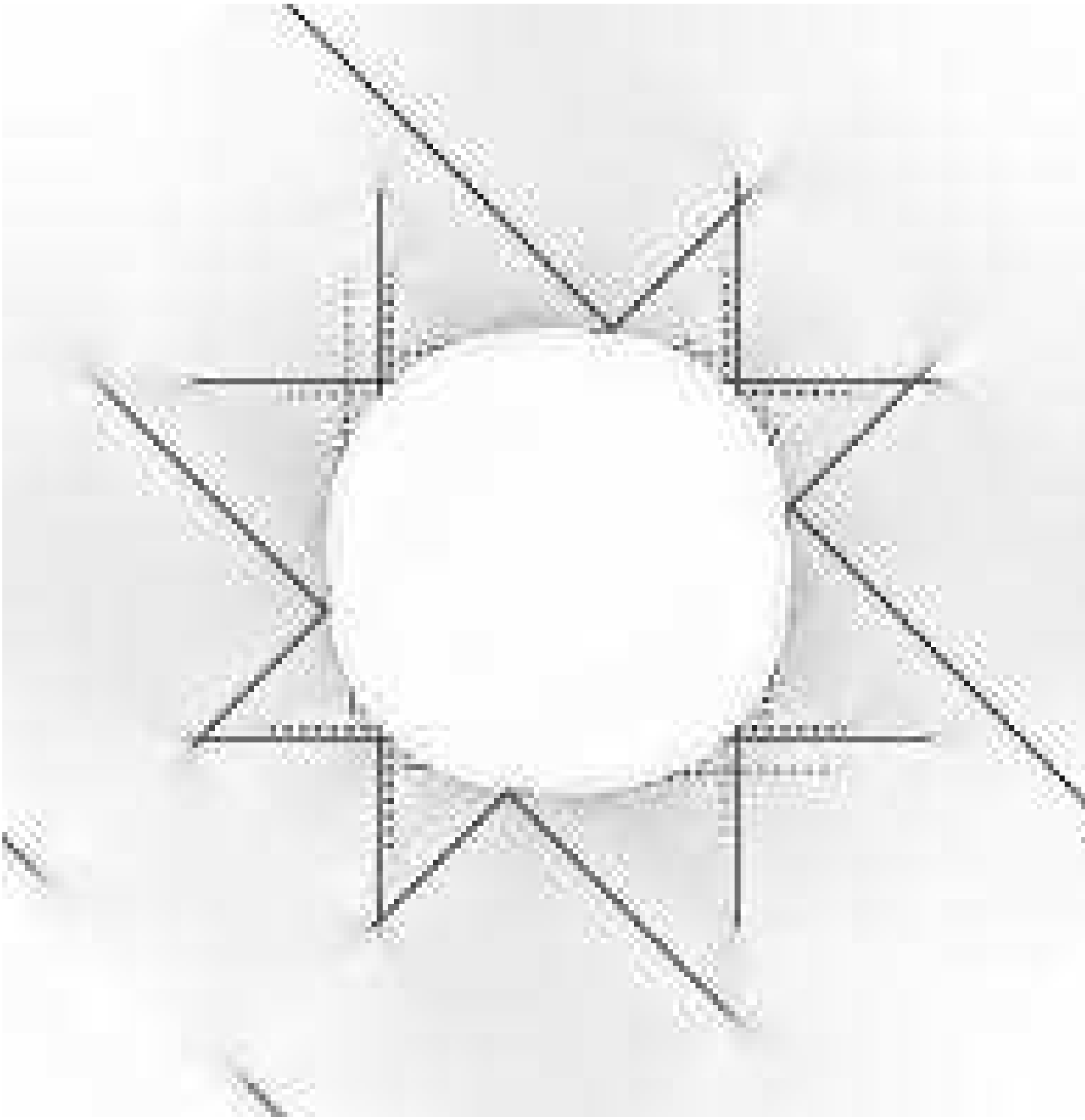

FIG. 6: Snapshot of e in (4.4) after dislocation formation, which is zero within the hard domain and nonvanishing outside. The slip lines end at dislocations.

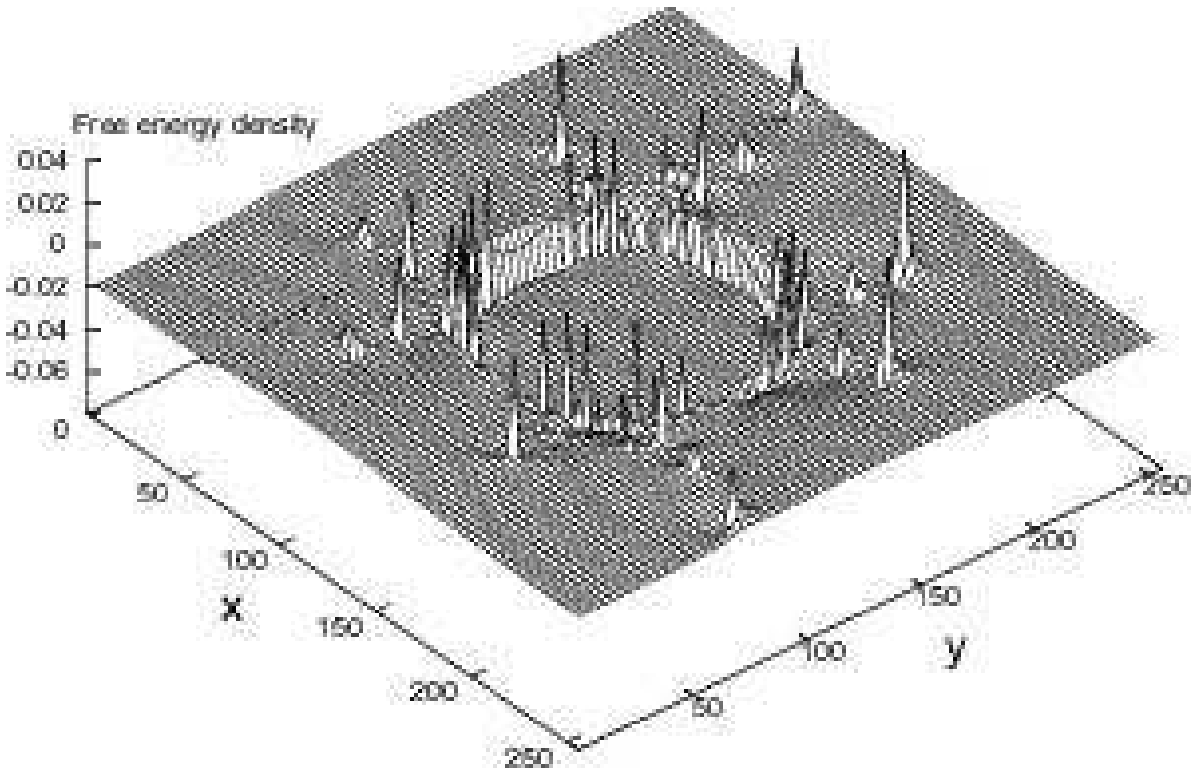

FIG. 7: Snapshot of the free energy density f in (2.3). The peaks are located near the dislocation cores and the cliff-like structure represents the interface free energy density.

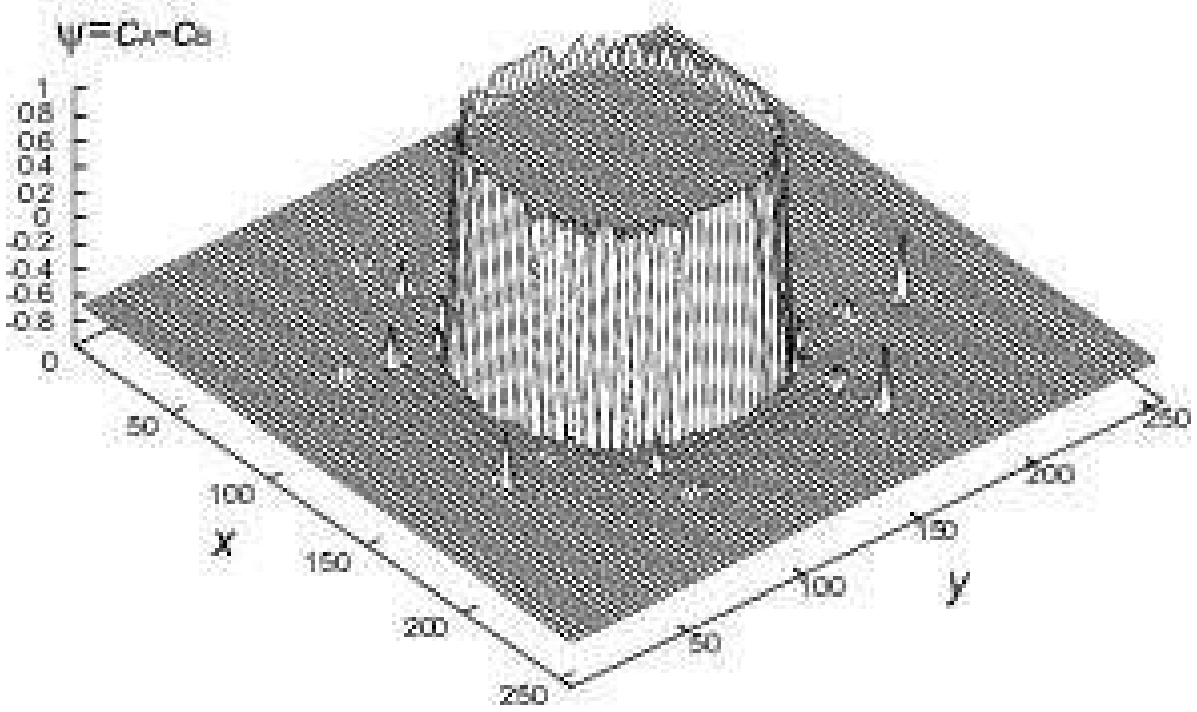

FIG. 8: Snapshot of the order parameter around a hard domain in the incoherent case obtained after a two-step quench. The peak structure at the interface arises because the system away from the interface is still in a transient state. The peaks around the dislocation cores in the outer soft region represent Cottrell atmospheres (but the minima paired are not seen in the figure).

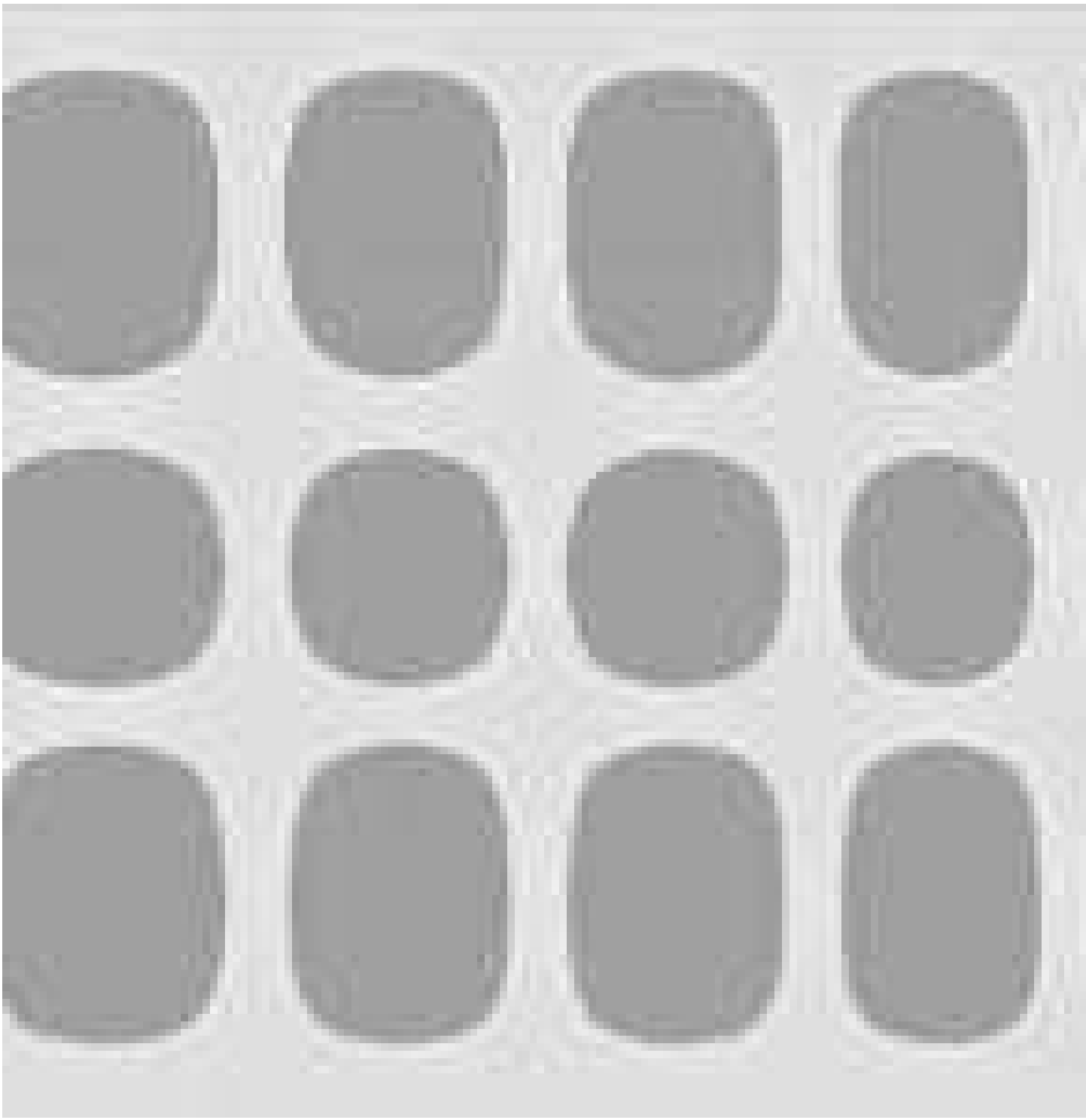

FIG. 9: Domain structure obtained at a shall quench $T/T_0 = 2$ in the coherent condition.

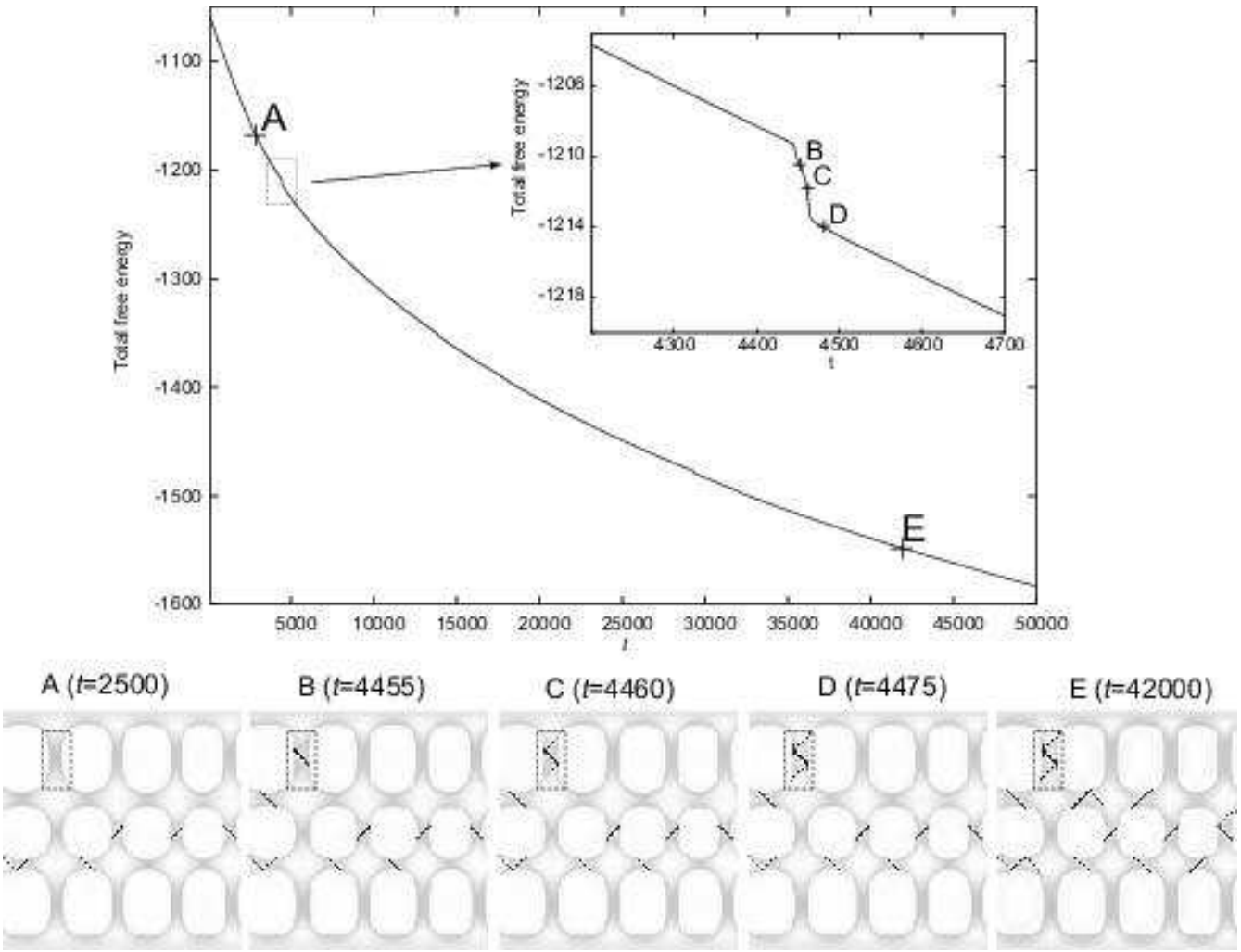

FIG. 10: Relaxation of the total free energy F in units of $\mu_{20}v_0 = 20k_{\rm B}T_0$ after a two-stepnch from $T/T_0 = 2$ to 1 with the initial configuration in Fig.9. It mostly relaxes due to the gradual composition adjustment, but it sometimes relaxed due to dislocation formation as enlarged in the inset. Snapshots of e at the points A $\sim$ E are given in the lower plates.

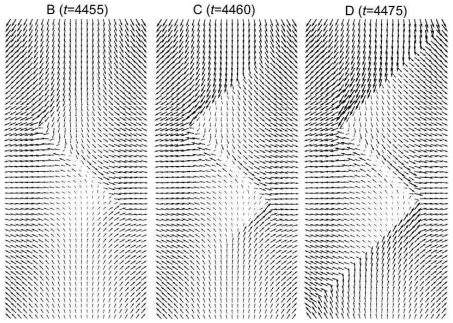

FIG. 11: Elastic displacement $\boldsymbol{u}$ in the marked regions B,C, and D.

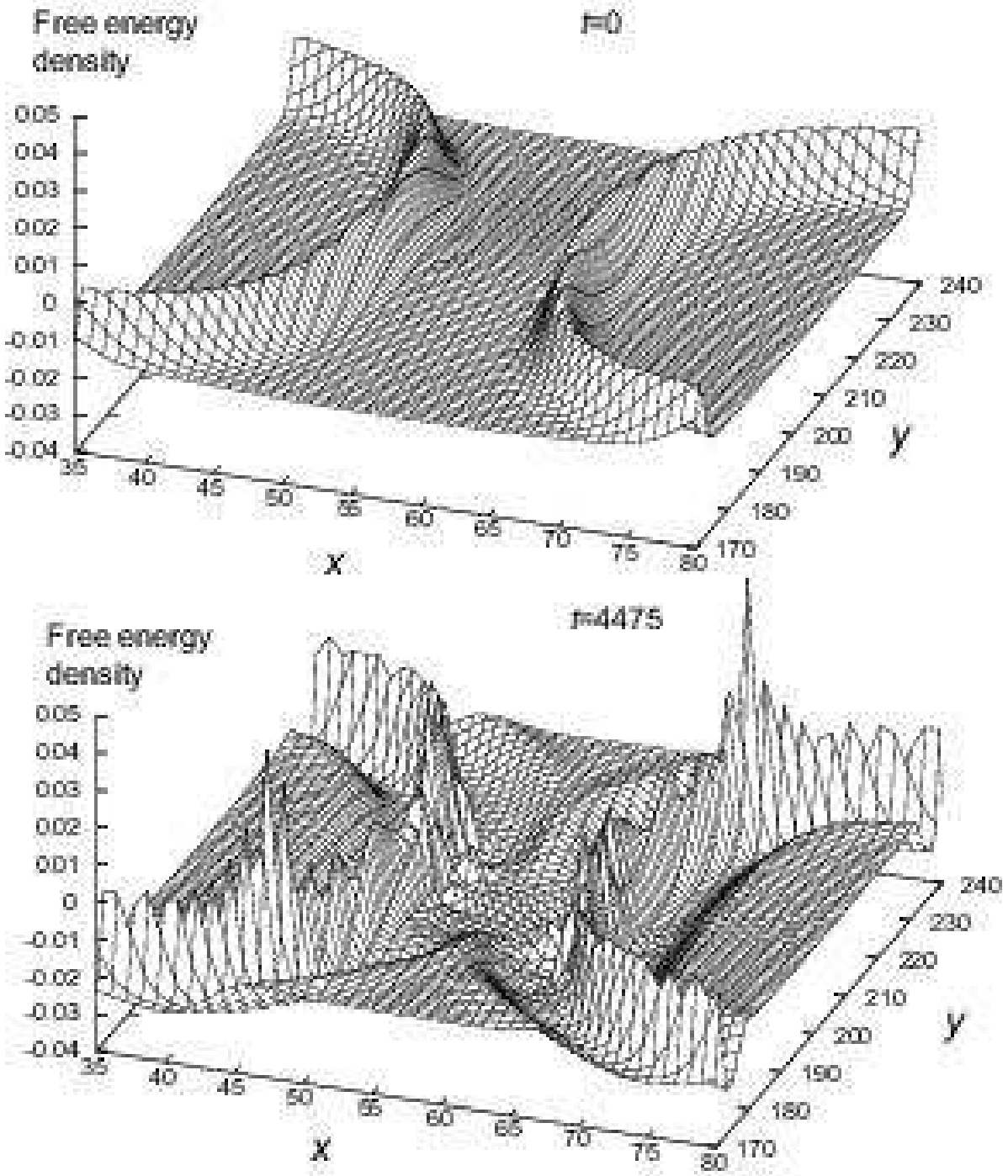

FIG. 12: Bird views of the free energy density f in units of $\mu_{20} = 20k_{\rm B}T_0v_0^{-1}$ at $t = 0$ and 4475 after the two-step quench in Fig.10.

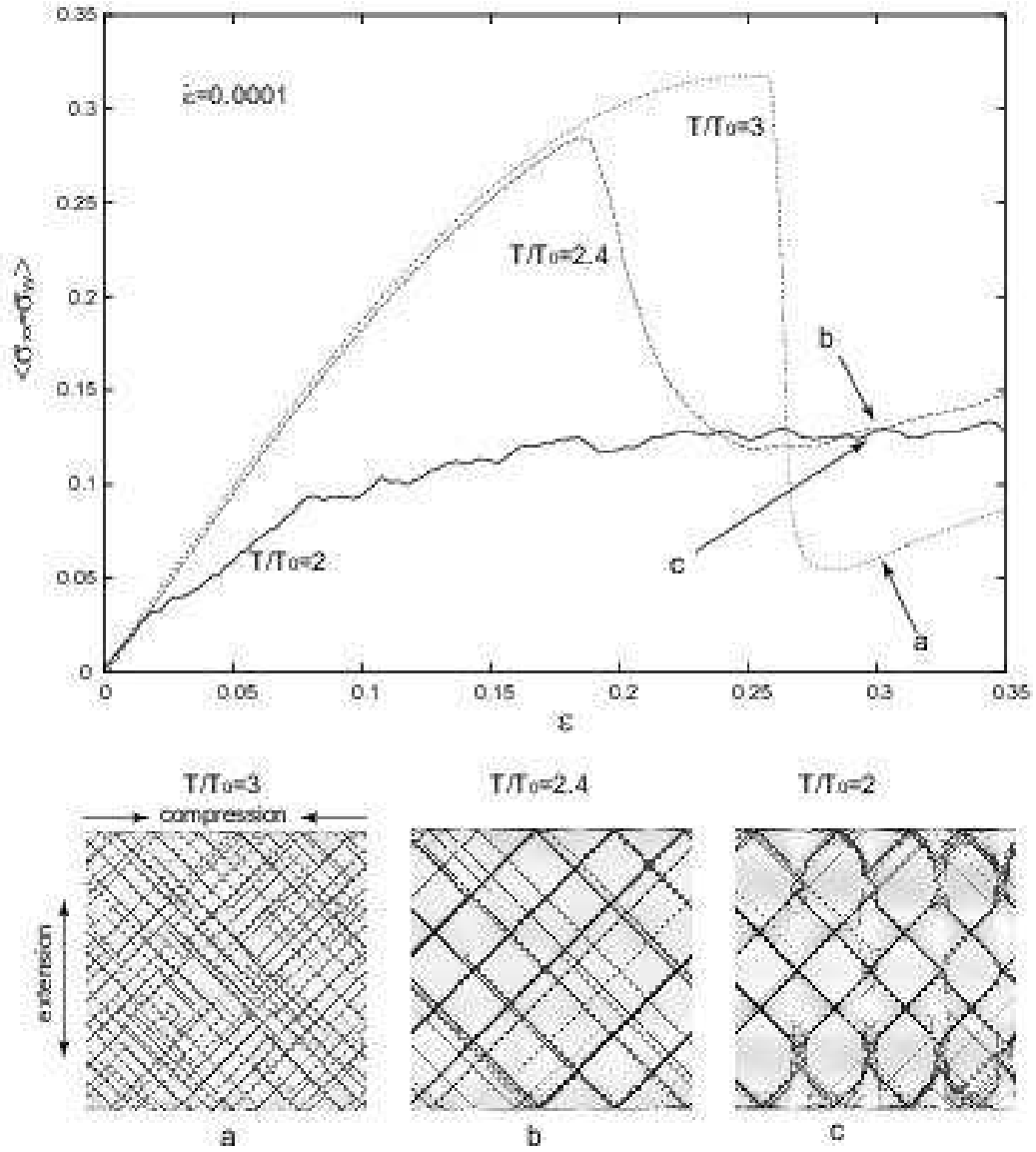

FIG. 13: Stress-strain curves after application of uniaxial stretching $\epsilon = \dot{\epsilon}t$ with $\dot{\epsilon} = 10^{-4}$ for $T/T_0 = 3, 2.4$, and 2. There is no dislocation at $t = 0$. Snapshots of e in (4.4) at points a,b, and c are given below, which represent slip patterns in plastic flow.

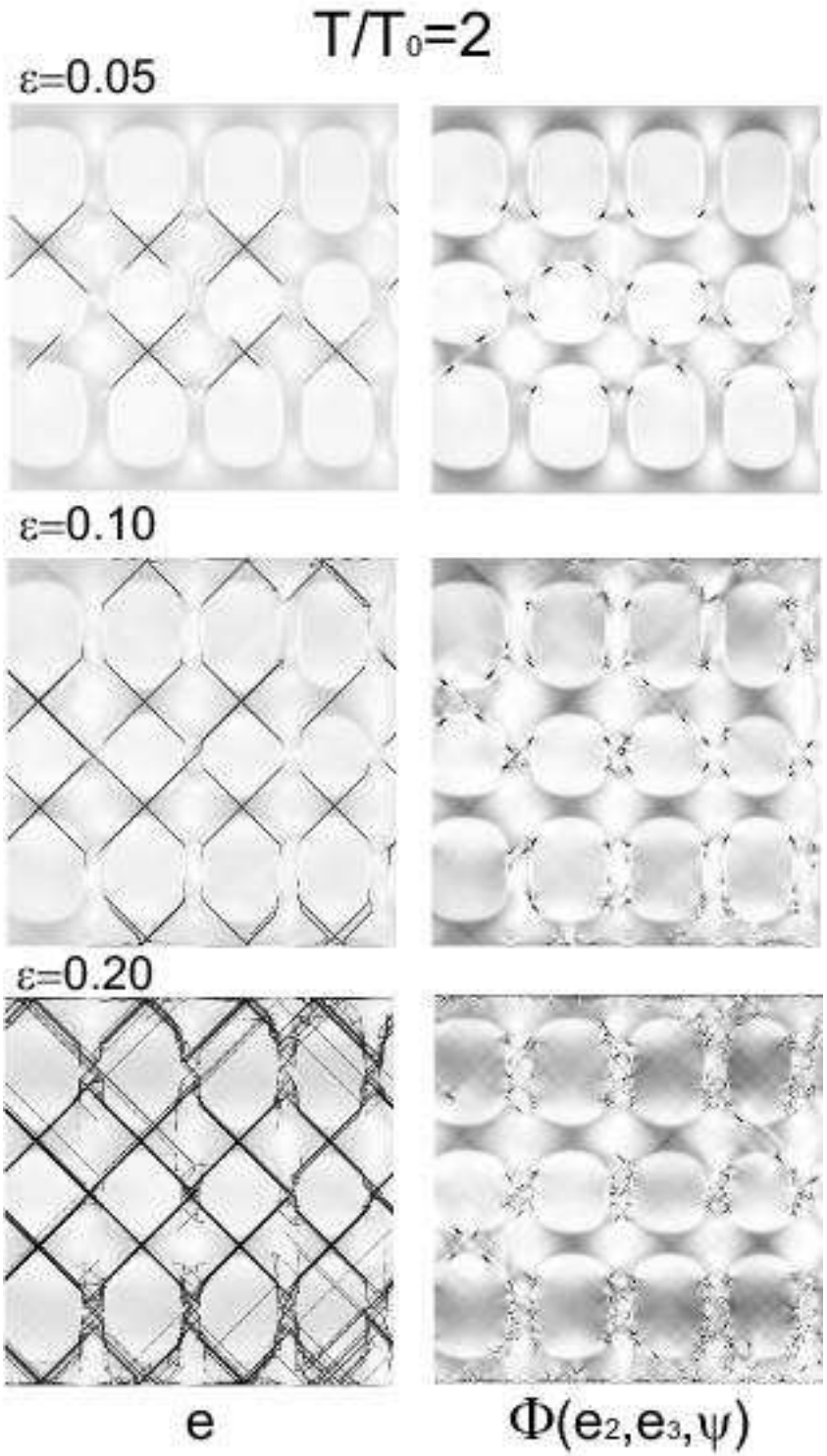

FIG. 14: Snapshots of e in (4.4) and the shear deformation energy density Φ in (2.7) at $T/T_0 = 2$ for $\epsilon = 0.05, 0.1,$ and 0.2.